Research Square

Preprints are preliminary reports that have not undergone peer review.
They should not be considered conclusive, used to inform clinical practice,
or referenced by the media as validated information.

Probiotic extracellular vesicles loaded with multifunctional nanozymes for inflammatory bowel disease treatment

Tingting Zhu
Nanjing Drum Tower Hospital
Guangtao Gao
Anhui Medical University
Zhiqiang Luo
Southeast University
Yuanjin Zhao
Southeast University
Guifang Xu
xuguifang@fy.ahmu.edu.cn

Nanjing Drum Tower Hospital

Research Article

Keywords: drug delivery, bimetallic nanozyme, probiotics, extracellular vesicle, inflammatory bowel disease

Posted Date: August 10th, 2026

DOI: https://doi.org/10.21203/rs.3.rs-10521481/v1

License: This work is licensed under a Creative Commons Attribution 4.0 International License.
Read Full License

Additional Declarations: No competing interests reported.

Abstract

Current therapies of inflammatory bowel disease (IBD) predominantly target single inflammatory pathways and often fail to resolve oxidative stress or restore mucosal homeostasis, resulting in suboptimal clinical outcomes. Here, we report a biomimetic nano-biohybrid platform that integrates multifunctional nanozymes with probiotic-derived extracellular vesicles for synergistic treatment of IBD. In this system, a Cu/Zn bimetallic nanozyme with superoxide dismutase- and catalase-mimetic activities is engineered to achieve efficient reactive oxygen species (ROS) scavenging, while extracellular vesicles derived from *Faecalibacterium prausnitzii* provide intrinsic intestinal targeting, mucus penetration capability, and immunomodulatory bioactivity. Thus, in a colitis model, the hybrid system markedly alleviates disease severity, as evidenced by improved body weight recovery, reduced disease activity index (DAI), and restoration of colon length. In addition, this treatment significantly suppresses ROS accumulation, downregulates pro-inflammatory cytokines, and promotes epithelial barrier repair by upregulating tight junction proteins. These results indicated that our work establishes a multifunctional therapeutic strategy that integrates nanocatalytic ROS regulation with microbiota-derived biological signaling, providing a promising platform for precision intervention in IBD and other inflammation-associated diseases.

1. Introduction

Inflammatory bowel disease (IBD), encompassing ulcerative colitis and Crohn's disease, is a chronic relapsing disorder of the gastrointestinal tract[1–3]. Despite extensive investigation, its pathogenesis remains incompletely understood. Accumulating evidence has identified excessive reactive oxygen species (ROS) and gut microbiota dysbiosis as central drivers of disease progression[2, 4]. Aberrant ROS accumulation disrupts intestinal epithelial barrier integrity, induces oxidative damage, and amplifies pro-inflammatory signaling cascades, thereby perpetuating mucosal inflammation and impairing tissue repair[5–7]. Meanwhile, microbial imbalance further exacerbates immune dysregulation, forming a vicious cycle that sustains chronic intestinal injury. Current therapeutic strategies, including amino salicylates, corticosteroids, immunosuppressants, and biologics such as anti-tumor necrosis factor (TNF) antibodies, can induce remission in a subset of patients. Nevertheless, their long-term clinical efficacy is often compromised by primary or secondary non-responsiveness, systemic adverse effects, and substantial economic burden[8, 9]. In addition, most existing treatments are designed to target single inflammatory pathways and fail to effectively eliminate excessive ROS, which is a key barrier to mucosal healing[10–12]. Therefore, there is an urgent need to develop integrated therapeutic strategies capable of simultaneously modulating oxidative stress, immune responses, and microbial homeostasis.

Here, we propose a novel biomimetic nano-biohybrid platform that integrates multifunctional nanozymes with probiotic-derived extracellular vesicles (EVs) for the treatment of IBD (Fig. 1). Nanozymes, a class of nanomaterials with enzyme-like catalytic activities, have emerged as promising regulators of oxidative stress. They can mimic the activities of natural enzymes, including superoxide dismutase (SOD), catalase (CAT), and peroxidase (POD), enabling efficient scavenging of ROS[13–16]. Compared with

natural enzymes, nanozymes exhibit superior stability, tunable catalytic properties, lower production cost, and flexible structural design[17–19]. However, conventional nanozymes suffer from poor intestinal targeting and limited retention at inflamed sites, which significantly restricts their therapeutic efficacy in IBD[20–22]. In contrast, extracellular vesicles, particularly those derived from probiotics, offer a complementary solution[23, 24]. These vesicles possess intrinsic intestinal tropism, the ability to penetrate the mucus barrier, and natural affinity for various intestinal immune cells[25]. In addition, they carry bioactive molecules that can modulate host immune responses and microbiota-related signaling pathways[26–28]. Such unique biological properties make probiotic EVs an ideal platform for targeted delivery and immunomodulation. We therefore hypothesize that integrating nanozymes with probiotic EVs enable synergistic regulation of oxidative stress and immune–microbiota interactions, thereby achieving enhanced therapeutic outcomes in IBD.

To validate this concept, we fabricated the desired biomimetic nano-biohybrid system by coupling a Cu/Zn bimetallic nanozyme with extracellular vesicles derived from *Faecalibacterium prausnitzii* (*F. prausnitzii*). The nanozyme component provides robust enzyme-mimetic catalytic activity for efficient ROS scavenging, while macrophage membrane cloaking enhances inflammatory targeting and immune compatibility. Through bio-orthogonal conjugation, the nanozyme is integrated with bacterial EVs, enabling coordinated modulation of host oxidative stress and microbiota-associated signaling. This multifunctional design confers several advantages in the biological experiments, including synergistic anti-inflammatory effects, restoration of gut microbial balance, and improved targeting efficiency and biosafety. Collectively, this study establishes a versatile therapeutic strategy that bridges nanocatalysis with microbiota-derived bioactivity, offering a promising avenue for precision treatment of IBD.

2. RESULTS AND DISCCUSSION

Preparation and characterization of CuZn-EVs

The biomimetic nano-biohybrid platform of CuZn-EVs was rationally engineered by integrating CuZn bimetallic nanozymes, macrophage membrane vesicles, and *F. prausnitzii*-derived EVs (*F.p*-EVs), as illustrated in Fig. 2A. Specifically, CuZn bimetallic metal-organic framework nanozymes were synthesized through a one-pot coordination assembly of Zn^{2+}, Cu^{2+}, and 2-methylimidazole [29], which employed ZIF-8, a kind of typical Zn metal–organic framework nanoparticles, as the framework. After incorporation of Cu^{2+} into the framework of ZIF-8, the resultant CuZn nanoparticles largely preserved the original polyhedral morphology and framework integrity of ZIF-8, as observed under Transmission electron microscopy (TEM) (Fig. 2B). Subsequently, macrophage membrane coating was introduced on the surface of CuZn nanozymes by ultrasound fusion method to confer inflammation-homing capability, obtained CuZn@CM nanoparticles. After membrane coating, a distinguishable shell-like corona surrounding the CuZn nanozymes became apparent, suggesting successful membrane encapsulation (Fig. 2B). In contrast, EVs with immunomodulatory functions were isolated from *F. prausnitzii* by ultracentrifugation. They exhibited characteristic vesicular structures. CuZn@CM nanoparticles were then conjugated with *F.p*-EVs by bioorthogonal click reaction, harvesting the final CuZn-EVs, which would

inherit the probiotic-associated immunomodulatory functions of *F. prausnitzii* [30]. The resultant CuZn-EVs retained both the electron-dense inorganic core and membrane-associated outer layer, confirming the successful integration of nanozymes and EVs, as observed under TEM.

Dynamic light scattering (DLS) measurements demonstrated the progressive changes in hydrodynamic diameter throughout the fabrication process (Fig. 2C and Figure S1A–D). Compared with initial CuZn nanozymes, membrane-coated CuZn@CM and EVs exhibited smaller average hydrodynamic particle sizes, whereas the final CuZn-EVs displayed an increased hydrodynamic diameter, consistent with successful hybridization between EVs and CuZn@CM. Correspondingly, zeta potential measurements revealed the distinct surface charge transitions during each modification step (Fig. 2D and Figure S1E–H). Additionally, all the nanoparticles exhibited uniform particle size distributions accompanied by low polydispersity index (PDI) values (< 0.3), indicating favorable colloidal homogeneity (Fig. 2E). Notably, CuZn-EVs maintained nearly unchanged particle size and PDI over 48 h of storage in aqueous solution (Fig. 2F), demonstrating excellent physicochemical stability. The elemental distribution analysis from energy-dispersive spectroscopy (EDS) mapping also supported the successful fabrication of CuZn-EVs. The element signals of O, P that is a characteristic component of phospholipid bilayers, and Zn that is the distinct element in CuZn nanozymes, were homogeneously distributed throughout the nanoparticles (Fig. 2G).

The chemical structure of the synthesized nanozymes was subsequently characterized by X-ray diffraction (XRD), Fourier-transform infrared (FTIR) spectroscopy, and X-ray photoelectron spectroscopy (XPS). FTIR spectrum demonstrated that the characteristic imidazolate-associated vibrational bands of ZIF-8 were largely preserved after Cu incorporation, indicating maintenance of the ZIF-8 derived coordination framework (Fig. 2H). XRD patterns further revealed that CuZn nanozymes retained the major diffraction peaks of ZIF-8, with only slight peak broadening and intensity attenuation (Fig. 2I), suggesting successful bimetallic engineering while preserving overall crystallinity. The chemical states and elemental composition were further examined by XPS (Fig. 2J–K and Figure S2A–D). Compared with ZIF-8, CuZn nanozymes exhibited additional Cu-related signals in the survey spectrum, confirming successful copper incorporation. High-resolution Zn 2p and Cu 2p spectra collectively verified the formation of a stable Cu/Zn bimetallic coordination network while preserving the imidazole-derived chemical architecture of the parent nanozymes. These results, together with FTIR and XRD analysis, also confirmed the successful construction of a structurally intact CuZn bimetallic nanozyme. In general, the CuZn nanozymes with ROS scavenging, macrophage membrane vesicles with biomimetic immune targeting, and *F.p*-EVs with microbiota-derived therapeutic activities were successfully incorporated within a single nano system by hierarchical assembly strategy. Benefiting from its components and structure, it was expected to simultaneously alleviate oxidative stress, regulate intestinal inflammation, and improve biological targeting efficiency for IBD therapy.

The Multi-Enzyme Catalytic and ROS Scavenging Mechanisms of CuZn Nanozymes

The therapeutic mechanism of the CuZn nanozymes is illustrated in Fig. 3A. With integrating Cu and Zn as catalytic centers, CuZn nanozymes were expected to mimic both SOD and CAT, enabling cascade conversion of ROS into H_2O_2 and its subsequent decomposition into H_2O and O_2[29]. Such cascade catalysis activities is particularly advantageous for treatment of IBD, where excessive ROS accumulation drives epithelial injury, mitochondrial dysfunction, and chronic inflammation[4]. For proof of concept, the enzyme-mimetic activities of CuZn nanozymes were first evaluated *in vitro*. As shown in Fig. 3B, CuZn nanozymes markedly reduced the absorbance of superoxide-derived chromogenic products at a concentration-dependent and time-dependent manner, indicating efficient $O_2^{\bullet -}$ scavenging. Meanwhile, CuZn nanozymes exhibited robust CAT-like activity to accelerate H_2O_2 decomposition (Fig. 3C). Unlike conventional antioxidants that target a single ROS species, CuZn nanozymes simultaneously eliminated both $O_2^{\bullet -}$ and H_2O_2, thereby disrupting ROS amplification cascade reactions that were commonly observed in inflamed intestinal tissues.

The multifunction of CuZn nanozymes was then quantified by co-incubating with cells. Coating of macrophage membrane and conjunction with *F.p*-EVs may enhance the inflammation targeting and intracellular uptake of CuZn-EVs. For proof of concept, their cell uptake capacity was quantified. Fluorescence imaging of DiD-labeled nanozymes revealed substantially enhanced uptake of CuZn-EVs in both NCM460 epithelial cells and RAW264.7 macrophages, compared with free CuZn nanozymes (Figure S3A, B). This was attributed to the biomimetic membrane structure of EVs to cell membrane, which facilitated cellular interaction and endocytosis to enhance cellular antioxidant efficacy. CCK-8 assays further demonstrated excellent cytocompatibility of CuZn nanozymes to both NCM460 epithelial cells and RAW264.7 macrophages across a broad concentration range (Figure S3C, D). Furthermore, the protective effect of CuZn nanozymes to against oxidant stress for cells was quantified. The H_2O_2-induced oxidative injury was established on both NCM460 epithelial cells and RAW264.7 macrophages, and cell viability was detected as quantification indicator. The results demonstrated that CuZn nanozymes treatment markedly improved cell viability of NCM460 epithelial cells and RAW264.7 macrophages under oxidative stress conditions (Figure S3E, F). Additionally, given the pivotal role of ROS in inflammatory progression, intracellular ROS levels of cells were subsequently evaluated using DCFH-DA staining. Both H_2O_2 and lipopolysaccharide (LPS) stimulation induced pronounced ROS accumulation in RAW264.7 macrophages, whereas CuZn nanozymes treatment significantly decreased intracellular ROS at a dose-dependent manner (Fig. 3D–E). Excessive ROS is known to induce redox-sensitive inflammatory signaling, including the NF-κB pathway. Thus, efficient ROS elimination by CuZn nanozymes may suppress downstream inflammatory amplification[31].

Based on the facts that mitochondria are both major sources and targets of ROS, JC-1 staining was used to preliminarily evaluate mitochondrial function [32, 33]. LPS stimulation induced mitochondrial depolarization in RAW264.7 cells (Fig. 3F), whereas H_2O_2 exposure produced a similar effect in NCM460 epithelial cells (Figure S3G). In contrast, CuZn nanozymes treatment effectively restored mitochondrial membrane potential, indicating preservation of mitochondrial integrity. This mitochondrial protection effect may further reduce secondary ROS production and reinforce intracellular redox homeostasis. Since epithelial barrier dysfunction is a central driver of IBD progression, the protective effect of CuZn

nanozyme on epithelial barrier function was also investigated by ZO-1 immunofluorescence staining. The results revealed that oxidative stress severely disrupted ZO-1 continuity and tight-junction organization of Caco-2 cells, whereas CuZn nanozymes restored ZO-1 expression and junctional integrity when its concentration reached 10 μg/mL (Fig. 3G). The preservation of CuZn nanozymes to tight-junction architecture would represent an important therapeutic mechanism of IBD treatment.

We next examined whether redox regulation of CuZn nanozymes could influence macrophage polarization. LPS treatment significantly upregulated the expression of proinflammatory M1 marker CD86 (Fig. 3H). Conversely, expression of the M2 marker CD206 was substantially elevated while the expression of CD86 was markedly inhibited, after CuZn nanozyme treatment (Fig. 3I). These findings suggest that CuZn nanozyme promoted macrophage polarization toward a reparative phenotype to attenuate inflammatory activation.

Collectively, CuZn nanozyme exhibited potent SOD-like and CAT-like catalytic activities, efficient intracellular ROS scavenging property, mitochondrial protective effects, epithelial barrier-preserving capacity, and macrophage reprogramming activity. These synergistic properties enable CuZn-EVs to interrupt the oxidative stress–inflammation cycle, providing a strong mechanistic basis for subsequent *in vivo* therapy against IBD.

In Vivo Biosafety and Inflammation-Responsive Colon Targeting of CuZn-EVs

The *in vivo* biosafety of CuZn-EVs was initially assessed after their oral administration. Histological staining results of major organs showed that no obvious pathological changes, inflammatory infiltration, or tissue injury occurred on the organs of mice, demonstrating their excellent systemic biocompatibility and negligible *in vivo* toxicity for oral therapeutic applications (Fig. 4A). Subsequently, the gastrointestinal distribution of CuZn-EVs that was labeled by fluorescent molecule DiR was checked under *in vivo* imaging system. In healthy mice, fluorescence signals from both CuZn nanozymes and CuZn-EVs gradually diminished over time because of normal gastrointestinal clearance (Fig. 4B). CuZn-EVs with EVs functionalization showed somewhat improvement of the colonic retention. When they were applied to the dextran sulfate sodium (DSS)-treated mice, CuZn-EVs exhibited markedly enhanced accumulation and prolonged residence within the inflamed colon than free CuZn nanozymes. *Ex vivo* imaging results of digestive tract and gastrointestinal tissues demonstrated that, compared with free CuZn nanozymes, CuZn-EVs displayed substantially stronger fluorescence signals throughout the digestive tract, particularly in the colon of DSS-treated mice (Fig. 4C, D). Consistently, markedly enhanced DiR fluorescence was also observed in the colon tissue sections after CuZn-EVs treatment (Fig. 4E), which was induced by enhanced mucosal localization and retention of CuZn-EVs. These findings demonstrated the abilities of probiotic EVs to facilitate inflammation-targeted localization and sustained retention of nanozymes at diseased intestinal sites. Additionally, quantitative analysis of whole-body imaging, isolated digestive tissues, colon samples, and tissue sections further demonstrated significantly higher retention efficiency of CuZn-EVs under inflammatory conditions (Fig. 4F, G). The enhanced intestinal accumulation of CuZn-EVs is likely attributable to the biomimetic properties of

probiotic-derived extracellular vesicles, which promote mucus adhesion and interaction with inflamed mucosa[34, 35]. In addition, increased epithelial permeability in DSS-induced colitis may facilitate local retention of CuZn-EVs within diseased tissues. Collectively, these findings demonstrate that CuZn-EVs possess excellent biosafety and inflammation-responsive colon-targeting properties, providing a favorable pharmacokinetic basis for colitis treatments.

CuZn-EVs Effectively Ameliorate Colitis on Murine Model.

The therapeutic efficacy of CuZn-EVs was evaluated in a DSS-induced acute colitis model following preliminary dose optimization of CuZn nanozymes (Figure S4A-F). DSS administration induced progressive reduced body weight, shortened colon length, elevated DAI and systemic inflammatory responses, whereas CuZn nanozymes treatment alleviated these pathological manifestations even at a lower dosage. Based on the overall therapeutic performance, 10 μg/g/d was selected for subsequent studies. The engineering of *F.p*-EVs onto the surface of CuZn nanozymes, namely CuZn-EVs, was expected to enhance their intestinal targeting and local retention. As illustrated in Fig. 5A, compared with EVs and CuZn nanozymes alone, oral administration of CuZn-EVs markedly attenuated disease progression in DSS-treated mice, preserving body weight and reducing DAI throughout disease development (Fig. 5B–D, Figure S5A). This result indicated a synergistic therapeutic effect between probiotic EVs and CuZn nanozymes. Colon shortening is another characteristic feature of DSS-induced colitis and reflects the severity of intestinal inflammation. While DSS treatment resulted in substantial colon contraction, CuZn-EVs treatment significantly restored the colon length of DSS-treated mice to levels approaching those of healthy controls (Fig. 5E, F). Notably, CuZn-EVs even showed better therapeutic efficacy than 5-ASA, a first-line clinical agent. Meanwhile, CuZn-EVs also markedly preserved mucosal architecture and reduced histological injury scores of mice while widespread epithelial damage, loss of crypts, and inflammatory cells infiltration were observed in DSS-treated mice (Fig. 5G, H).

Epithelial barrier dysfunction, featured with loss of tight-junction integrity, is essential pathogenesis of colitis. To checked the protection capacity of CuZn-EVs to the epithelial barrier, the expression of ZO-1 and Occludin was assessed[36]. DSS exposure caused a profound decreased expression of ZO-1 and Occludin, reflecting significant impairment of epithelial barrier function. In contrast, CuZn-EVs treatment substantially restored the expression of both these two proteins to near-normal levels in DSS-treated mice (Fig. 5I–L). Given the potent enzyme-mimetic activity of CuZn-EVs, oxidative stress-related parameters were further examined. DSS treatment markedly impaired total antioxidant capacity (T-AOC) in colonic tissues, whereas CuZn-EVs treatment significantly restored T-AOC levels (Figure S5D). Consistent results were obtained by western blotting (Figure S5E), confirming effective reconstruction of epithelial barrier integrity. Restoration of tight-junction architecture is expected to limit luminal antigen translocation and thereby suppress chronic mucosal inflammation. CuZn-EVs treatment markedly restored DSS-induced reduction of Ki-67 expression in colonic crypts, indicating enhanced epithelial proliferation and mucosal repair (Figure S5F, G). Consistent with these findings, immunostaining of 4-HNE revealed extensive oxidative damage in DSS-treated colons, whereas CuZn-EVs treatment dramatically decreased 4-HNE accumulation (Figure S5H, I). Importantly, the antioxidative efficacy of

CuZn-EVs exceeded that of EVs or CuZn nanozymes monotherapy, highlighting the advantages of EVs-mediated intestinal targeting and prolonged local nanozyme retention. Collectively, EVs conjugation enhanced the intestinal accumulation of CuZn nanozymes and amplified their therapeutic activity within inflamed tissues. CuZn-EVs effectively alleviated colitis by simultaneously suppressing oxidative stress, reducing inflammatory infiltration, restoring epithelial barrier integrity, and promoting mucosal repair, providing a promising nano-biohybrid strategy for IBD treatment.

Anti-IBD Mechanism of CuZn@EVs in vivo

To investigate the immunomodulatory mechanisms responsible for the therapeutic effects of CuZn-EVs, systemic inflammatory responses and colonic immune remodeling in DSS-induced colitis model were comprehensively evaluated. In mice with DSS-induced colitis, marked leukocytosis and lymphocytosis, together with reductions in red blood cells (RBC) and HGB levels were observed, reflecting their severe systemic inflammation and intestinal bleeding. In contrast, CuZn-EVs treatment significantly normalized these hematological abnormalities and exhibited superior therapeutic efficacy, compared with EVs or CuZn nanozymes alone (Fig. 6A–D, Figure S5B, C). At the tissue level, DSS treatment markedly elevated the levels of TNF-α and IL-6, accompanied by a pronounced reduction in the anti-inflammatory factors IL-10 and TGF-β. CuZn-EVs effectively reversed these changes, indicating restoration of local immune homeostasis (Fig. 6E–J). In addition, macrophage polarization plays a vital role in inflammation response. Colitis resulted in a marked increase in M1 macrophage infiltration, whereas CuZn-EVs markedly reduced M1 polarization and enhanced the abundance of M2 macrophages (Fig. 6K–N). Consistently, inflammatory cytokine profiling revealed broad suppression of TNF-α, IL-6, IL-1β, CXCL1, and CCL2, accompanied by recovery of anti-inflammatory factors, such as IL-4 and IL-10 (Fig. 6O).

These findings suggest that CuZn-EVs re-construct the intestinal immune microenvironment from a pro-inflammatory status toward a tissue-repairing status. Collectively, CuZn-EVs alleviate intestinal inflammation through coordinated suppression of inflammatory signaling and promotion of reparative macrophage polarization.

To further investigate the underlying molecular mechanisms of disease remission, transcriptomic and metabolomic analyses of colonic tissues were performed. Transcriptome profiling revealed extensive gene reprogramming after CuZn-EVs treatment, characterized by downregulation of inflammation-associated genes and restoration of genes involved in epithelial repair and tissue regeneration (Fig. 7A). GO enrichment analysis indicated significant regulation of genes related to extracellular matrix organization, cell adhesion, cytokine activity, and inflammatory responses (Fig. 7B), while KEGG analysis highlighted enrichment of cytokine–cytokine receptor interaction, PI3K-Akt, MAPK, ECM-receptor interaction, and FoxO signaling pathways (Fig. 7C). PCA and PLS-DA score plots revealed a clear separation between the CuZn-EVs and DSS groups, indicating that CuZn-EVs markedly reshaped the metabolic profile in DSS-induced colitis (Fig. 7D). Metabolomic analysis revealed significant restoration of metabolic homeostasis after CuZn-EVs treatments. The differential metabolites were predominantly associated with pathways including pantothenate and CoA biosynthesis, β-alanine metabolism,

galactose metabolism, amino sugar metabolism, and nucleotide metabolism (Fig. 7E–G). Notably, CuZn-EVs therapy increased several metabolites associated with antioxidant defense and intestinal health, including indole-3-propionic acid and salicylic acid, while reducing inflammation-associated metabolites. These findings indicate that CuZn-EVs simultaneously regulate inflammatory signaling, extracellular matrix remodeling, and metabolic adaptation, thereby creating a favorable microenvironment for mucosal recovery.

To examine microbial composition, 16S rRNA sequencing was employed to evaluate microbial alterations after CuZn-EVs treatment. DSS induction markedly reduced microbial richness and diversity, whereas CuZn-EVs significantly restored Feature richness, Shannon diversity, and phylogenetic diversity (Fig. 8A–C). Venn analysis further demonstrated an increased number of distinct operational taxonomic units (OTUs) in the CuZn-EVs group, suggesting reconstruction of a more diverse microbial ecosystem (Fig. 8D). Microbial community analysis revealed a distinct separation between healthy and DSS-treated mice, while CuZn-EVs shifted the microbial composition of DSS-treated mice toward the healthy state (Fig. 8E). Differential abundance analysis showed the enrichment of beneficial bacterial groups, involving *Muribaculaceae*, *Bifidobacteriaceae*, *Prevotellaceae*, and *Rikenellaceae*, together with partial normalization of DSS-induced alterations in Proteobacteria, Bacteroidota, and Firmicutes abundance (Fig. 8F–I). Compared with the DSS group, CuZn-EVs treatment significantly reshaped the gut microbiota composition, partially restoring the abundance of beneficial bacteria (e.g., Lactobacillus reuteri) and modulating opportunistic pathogenic taxa (Figure S6A-H). Consistent with these observations, LEfSe and heatmap analyses demonstrated that the microbiota profile of CuZn-EVs-treated mice was more closely resembled to that of healthy controls. Taken together, these findings suggest that CuZn-EVs not only suppress intestinal inflammation and oxidative stress but also restore host–microbiota homeostasis. Combined with transcriptomic and metabolomic reprogramming, microbiota remodeling constitutes an important mechanism contributing to the therapeutic efficacy of CuZn-EVs in colitis.

3. Conclusion

In summary, we developed a probiotic extracellular vesicle-engineered CuZn nanozyme platform (CuZn-EVs) for oral treatment of IBD. By integrating the ROS-scavenging activity of CuZn nanozymes with the inflammation-targeting and biomimetic properties of *F prausnitzii*-derived EVs, CuZn-EVs achieved enhanced accumulation and prolonged retention within inflamed intestinal tissues. They effectively mitigated DSS-induced colitis, preserved epithelial barrier function, and facilitated mucosal healing. In aspect of mechanism, CuZn-EVs disrupted the oxidative stress–inflammation cycle through efficient ROS elimination, restoration of antioxidant capacity, and suppression of lipid peroxidation. Meanwhile, CuZn-EVs reprogrammed the intestinal immune microenvironment by inhibiting pro-inflammatory cytokines production and favoring M2 macrophage polarization. Multi-omics analyses further revealed that CuZn-EVs remodeled inflammatory transcriptional networks, restored metabolic homeostasis, and reversed gut microbiota dysbiosis. The coordinated regulation of oxidative stress, immunity, metabolism, and host–microbiota interactions collectively contributed to intestinal homeostasis and disease remission. Overall, this study establishes a multifunctional nano-biohybrid therapeutic strategy that

combines nanozyme catalysis with probiotic extracellular vesicle engineering for precise modulation of the intestinal inflammatory microenvironment. These findings provide a promising oral nanotherapeutic approach for IBD and offer a general framework for developing next-generation nanomedicines targeting complex inflammatory diseases. Additionally, our work highlights the potential of integrating catalytic nanomedicine with microbiota-derived biointerfaces, providing a versatile platform for the treatment of inflammation-driven diseases through simultaneous regulation of oxidative stress, immunity, and host–microbiota crosstalk.

Declarations

Acknowledgements: This work was supported by grants from the National Natural Science Foundation of China (Grant Nos. 82300600, 82570625); the Nanjing Medical Science and Technology Development Program (Nos. ZKX23013, YKK12072, YKK15061 and YKK16078); Jiangsu Provincial Six Talent Peaks (WSN-078); Anhui Province Innovation Group Project (2025AHGXZK10002); Major Program of 2023 Taikang Xianlin Drum Tower Hospital Fund (no. TKKYZA20233001, TKKYYB20243006).

Conflict of Interest No conflicts of interest are disclosed by the writers.

Ethics Statement Ethics approval for experiments reported in the submitted manuscript on animal subjects was granted. The ethics has been approved by Nanjing Drum Tower Hospital, Affiliated Hospital of Medical School, Nanjing University. The ethical number is 2025AE01170.

Author Contributions: Guifang Xu and Yuanjin Zhao conceived the research and designed the experiments. Tingting Zhu and Guangtao Gao performed the experiments, analyzed corresponding data, and wrote the whole manuscript. Zhiqiang Luo contributed to the experimental operations and data discussions.

References

1. Danne C, et al. Neutrophils: from IBD to the gut microbiota. Nat Rev Gastroenterol Hepatol. 2024;21(3):184–97.
2. Zhou J, et al. Programmable probiotics modulate inflammation and gut microbiota for inflammatory bowel disease treatment after effective oral delivery. Nat Commun. 2022;13(1):3432.
3. Cao Y, et al. Commensal microbiota from patients with inflammatory bowel disease produce genotoxic metabolites. Science. 2022;378(6618):eabm3233.
4. Bhattacharyya A, et al. Oxidative stress: an essential factor in the pathogenesis of gastrointestinal mucosal diseases. Physiol Rev. 2014;94(2):329–54.
5. Iatsenko I, Boquete JP, Lemaitre B. Microbiota-Derived Lactate Activates Production of Reactive Oxygen Species by the Intestinal NADPH Oxidase Nox and Shortens Drosophila Lifespan. Immunity. 2018;49(5):929–e9425.

6. Sun Y, et al. The role of gut microbiota in intestinal disease: from an oxidative stress perspective. Front Microbiol. 2024;15:1328324.
7. Lee Y, et al. Hyaluronic acid-bilirubin nanomedicine for targeted modulation of dysregulated intestinal barrier, microbiome and immune responses in colitis. Nat Mater. 2020;19(1):118–26.
8. Neurath MF. Strategies for targeting cytokines in inflammatory bowel disease. Nat Rev Immunol. 2024;24(8):559–76.
9. Hashash JG, et al. Medical management of inflammatory bowel diseases. BMJ. 2025;391:e079050.
10. Bernstein CN, et al. World Gastroenterology Organization Practice Guidelines for the diagnosis and management of IBD in 2010. Inflamm Bowel Dis. 2010;16(1):112–24.
11. Zu M, et al. Oral delivery of natural active small molecules by polymeric nanoparticles for the treatment of inflammatory bowel diseases. Adv Drug Deliv Rev. 2021;176:113887.
12. Wan J, et al. Epidemiology, pathogenesis, diagnosis, and treatment of inflammatory bowel disease: Insights from the past two years. Chin Med J (Engl). 2025;138(7):763–76.
13. Ren X, et al. Nanozymes-recent development and biomedical applications. J Nanobiotechnol. 2022;20(1):92.
14. Zhang R, Fan K, Yan X. Nanozymes: created by learning from nature. Sci China Life Sci. 2020;63(8):1183–200.
15. Chen Z, et al. Rational Design Strategies for Nanozymes. ACS Nano. 2023;17(14):13062–80.
16. Perwez M, et al. Nanozymes and nanoflower: Physiochemical properties, mechanism and biomedical applications. Colloids Surf B Biointerfaces. 2023;225:113241.
17. Huang Y, Ren J, Qu X. Nanozymes: Classification, Catalytic Mechanisms, Activity Regulation, and Applications. Chem Rev. 2019;119(6):4357–412.
18. Wu J, et al. Nanomaterials with enzyme-like characteristics (nanozymes): next-generation artificial enzymes (II). Chem Soc Rev. 2019;48(4):1004–76.
19. Yang Y, et al. Nanozymes: Potential Therapies for Reactive Oxygen Species Overproduction and Inflammation in Ischemic Stroke and Traumatic Brain Injury. ACS Nano. 2024;18(26):16450–67.
20. Lei F, et al. Pathogenesis guided application of nanozymes in the treatment of inflammatory bowel disease. Mater Today Bio. 2025;33:102008.
21. Liu C, Wang Q, Wu YL. Recent Advances in Nanozyme-Based Materials for Inflammatory Bowel Disease. Macromol Biosci. 2023;23(10):e2300157.
22. Wu W, et al. Precise modulation of redox reactions: A novel multifunctional theranostic platform based on 2D nanozymes. Mater Today Bio. 2025;34:102255.
23. van Niel G, D'Angelo G, Raposo G. Shedding light on the cell biology of extracellular vesicles. Nat Rev Mol Cell Biol. 2018;19(4):213–28.
24. Marar C, Starich B, Wirtz D. Extracellular vesicles in immunomodulation and tumor progression. Nat Immunol. 2021;22(5):560–70.

25. Vader P et al. *Extracellular vesicles for drug delivery.* Adv Drug Deliv Rev, 2016. 106(Pt A): pp. 148–156.
26. Robbins PD, Morelli AE. Regulation of immune responses by extracellular vesicles. Nat Rev Immunol. 2014;14(3):195–208.
27. Buzas EI. The roles of extracellular vesicles in the immune system. Nat Rev Immunol. 2023;23(4):236–50.
28. Kalluri R. The biology and function of extracellular vesicles in immune response and immunity. Immunity. 2024;57(8):1752–68.
29. Huang F, et al. Dual-Site Biomimetic Cu/Zn-MOF for Atopic Dermatitis Catalytic Therapy via Suppressing FcγR-Mediated Phagocytosis. J Am Chem Soc. 2024;146(5):3186–99.
30. Pan Y, et al. Faecalibacterium Prausnitzii extracellular vesicles regulating macrophage differentiation via homologous recombination repair in colitis model. Microbiol Res. 2025;298:128217.
31. Morgan MJ, Liu ZG. Crosstalk of reactive oxygen species and NF-κB signaling. Cell Res. 2011;21(1):103–15.
32. Zorov DB, Juhaszova M, Sollott SJ. Mitochondrial reactive oxygen species (ROS) and ROS-induced ROS release. Physiol Rev. 2014;94(3):909–50.
33. Palma FR, et al. ROS production by mitochondria: function or dysfunction? Oncogene. 2024;43(5):295–303.
34. Domínguez Rubio AP, et al. Probiotics, Their Extracellular Vesicles and Infectious Diseases. Front Microbiol. 2022;13:864720.
35. Chen X, et al. Immunomodulatory Effects of Probiotic-Derived Extracellular Vesicles: Opportunities and Challenges. J Agric Food Chem. 2024;72(35):19259–73.
36. Cheng Y, et al. Targeting uPA-uPAR interaction to improve intestinal epithelial barrier integrity in inflammatory bowel disease. EBioMedicine. 2022;75:103758.

Figures

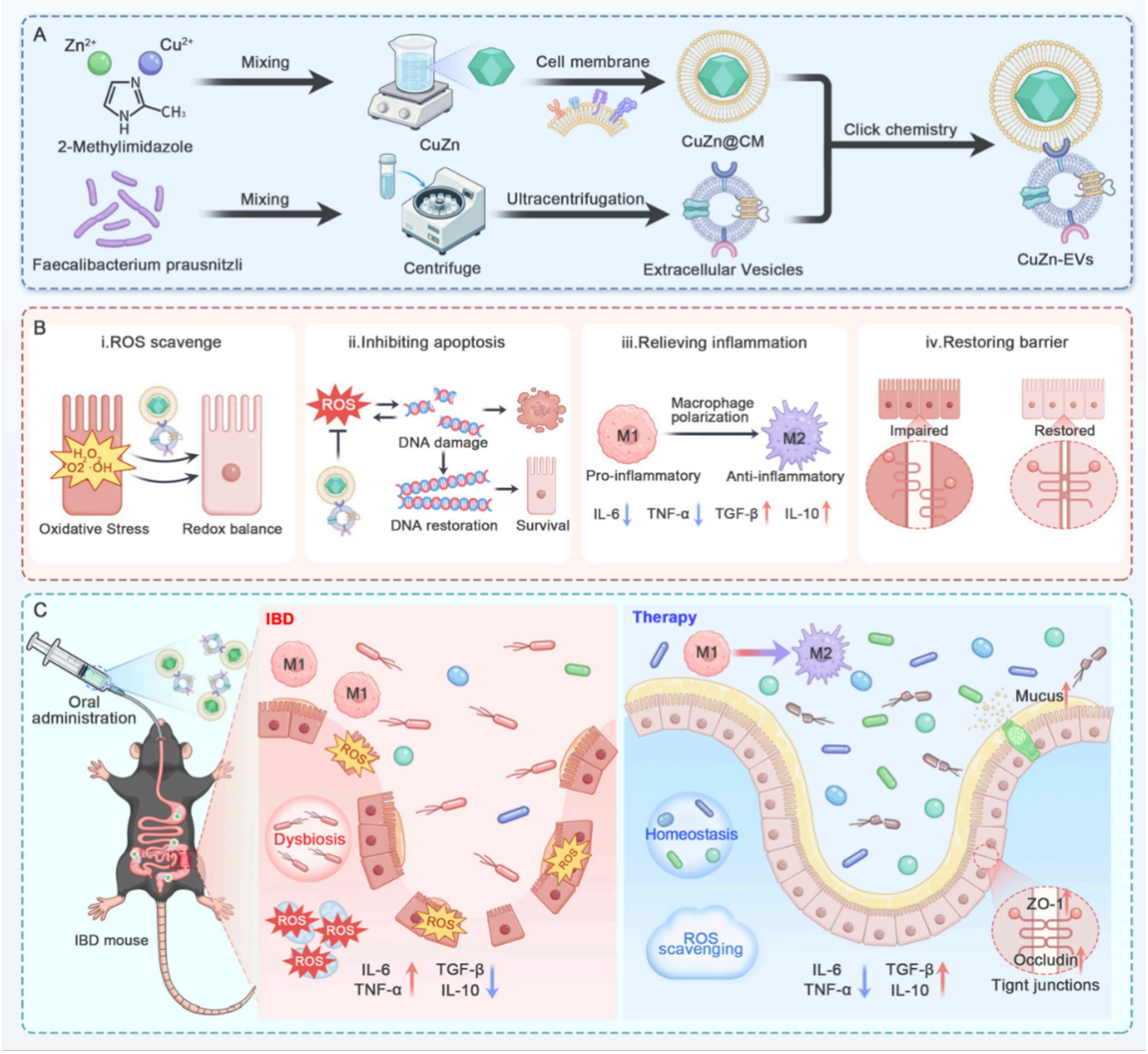


Figure 1

Diagram illustration of the preparation and therapeutic mechanisms of biohybrid CuZn-EVs for IBD treatment. (A) Schematic diagram of CuZn-EVs fabrication by integrating CuZn nanozymes with *F. prausnitzii*-derived EVs. (B) The main four therapeutic effects of CuZn-EVs. (C) The restoration of intestinal homeostasis via microbiota modulation, intestinal barrier repair, and immunoregulation.

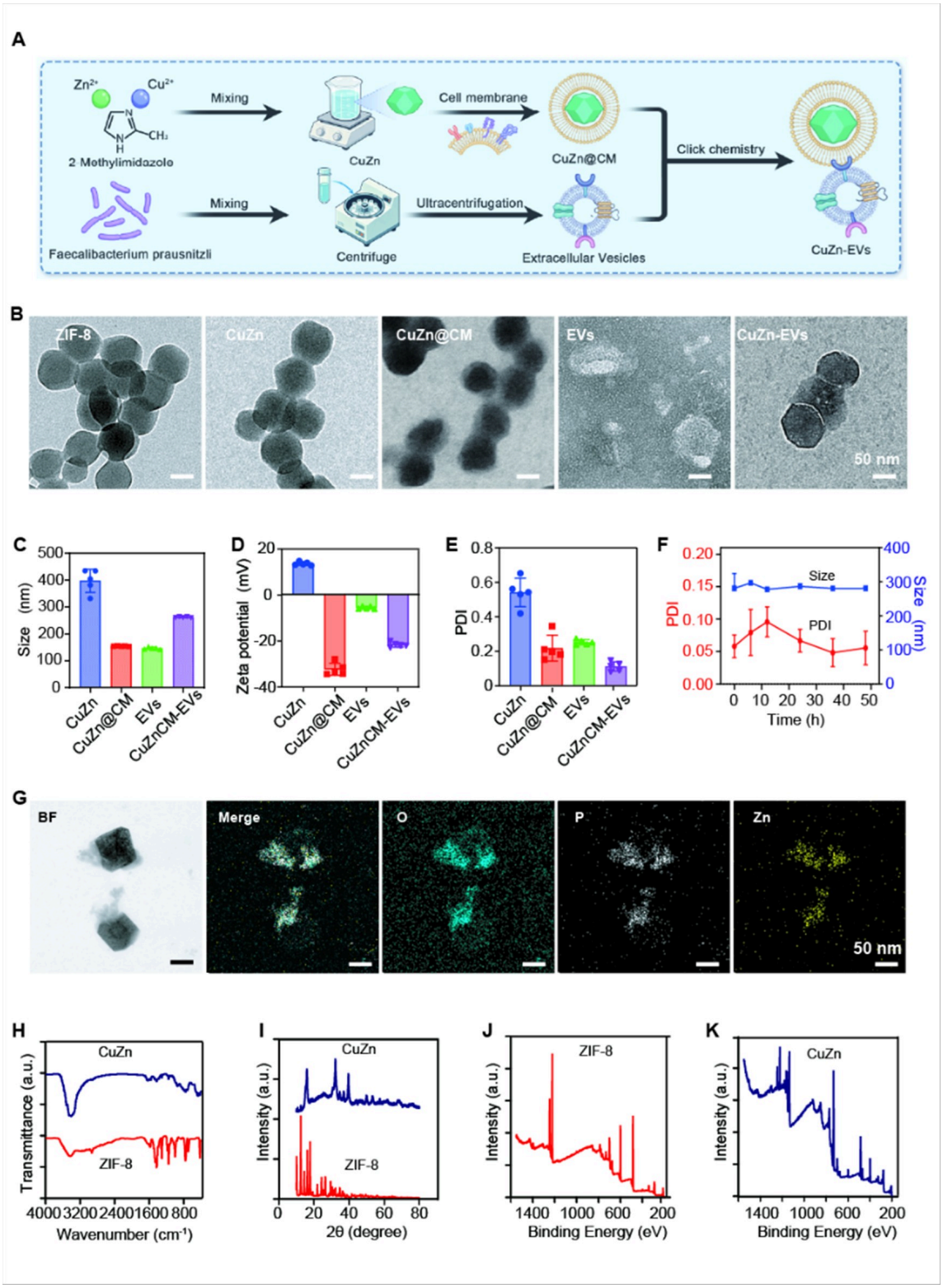


Figure 2

Fabrication and characterization of CuZn-EVs nano-biohybrid system.

(A) Schematic illustration of the preparation process of CuZn-EVs. (B) TEM images of ZIF-8, CuZn nanozyme, CuZn@CM, EVs, and CuZn-EVs. Scale bars, 50 nm. (C–E) Hydrodynamic size, zeta potential, and PDI analysis of CuZn nanozymes, CuZn@CM, EVs, and CuZn-EVs. (F) Stability analysis of CuZn-EVs

in aqueous solution over time, including hydrodynamic size and PDI measurements. (G) Elemental mapping analysis of CuZn-EVs showing the distribution of O, P, and Zn elements. Scale bars, 50 nm. (H) FTIR spectrum of ZIF-8 and CuZn nanozymes. (I) XRD patterns of ZIF-8 and CuZn nanozymes. (J–K) XPS survey spectra of ZIF-8 and CuZn nanozymes, respectively.

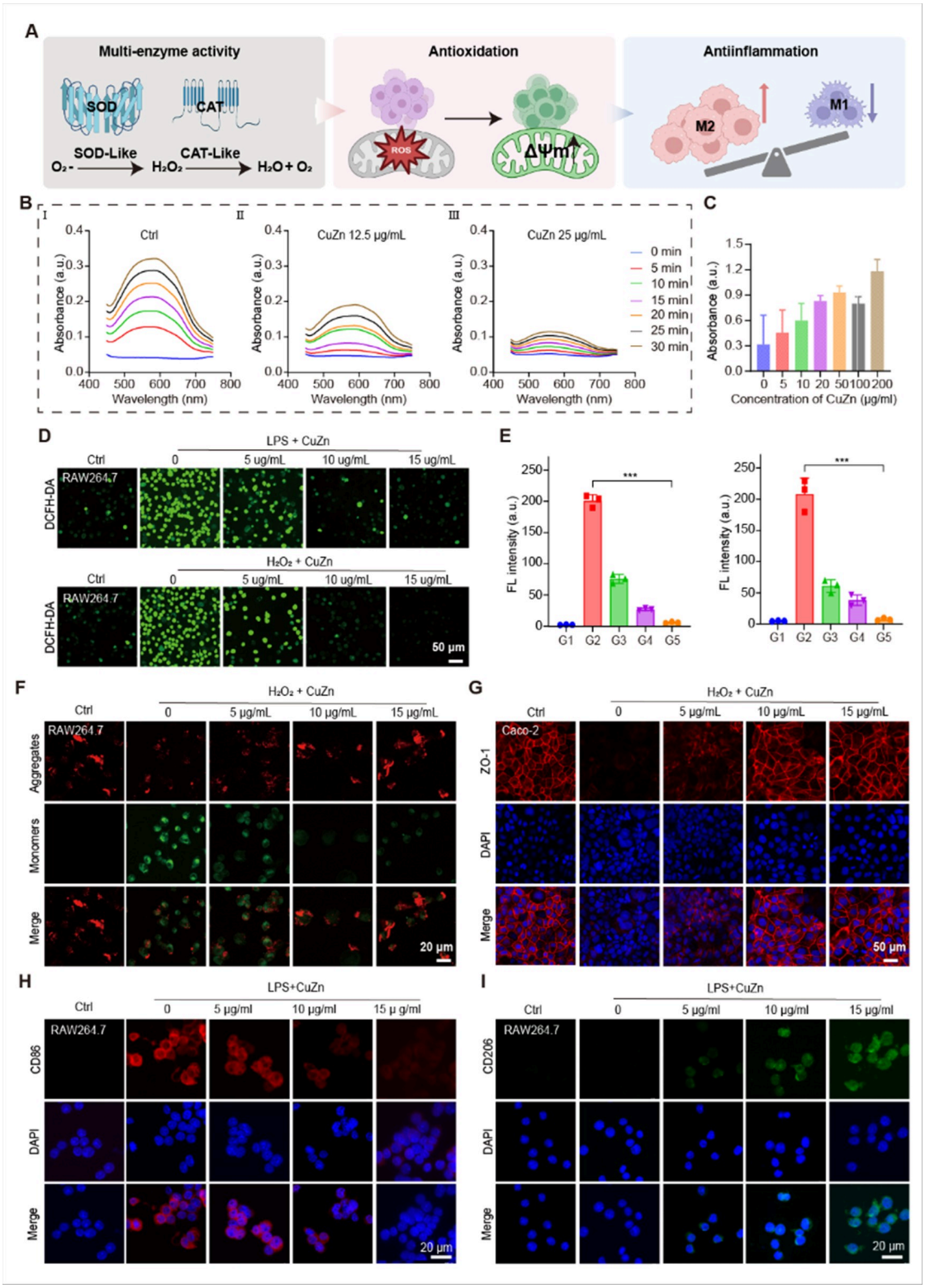


Figure 3

Antioxidant and anti-inflammatory activities of CuZn nanozymes *in vitro*.

(A) Schematic illustration of the multifunctional enzyme-like activities and biological effects of CuZn nanozymes, including SOD- and CAT-mimetic activities, ROS scavenging, mitochondrial protection, and macrophage polarization regulation. (B) SOD-like activity analysis of CuZn nanozymes at different concentrations measured by UV–vis spectroscopy. (C) Quantitative analysis of CAT-like activity of CuZn nanozymes at increasing concentrations. (D) Representative fluorescence images showing intracellular ROS levels in RAW264.7 macrophages after LPS and H_2O_2 stimulation and CuZn nanozymes treatment. Scale bars, 50 μm. (E) Quantification of intracellular ROS fluorescence intensity in RAW264.7 cells under LPS- (left) and H_2O_2- (right) induced oxidative stress conditions. (F) JC-1 staining analysis of mitochondrial membrane potential in RAW264.7 cells after different treatments. Red fluorescence indicates JC-1 aggregates, while green fluorescence indicates JC-1 monomers. Scale bars, 20 μm. (G) Immunofluorescence staining of tight junction protein ZO-1 in intestinal epithelial cells receiving H_2O_2-induced oxidative injury and CuZn nanozymes treatment. Scale bars, 50 μm. (H–I) Immunofluorescence staining of macrophage polarization markers CD86 and CD206 in RAW264.7 cells after LPS stimulation and CuZn nanozymes treatment. Scale bars, 20 μm. Data are presented as mean ± SD (*n*= 3).

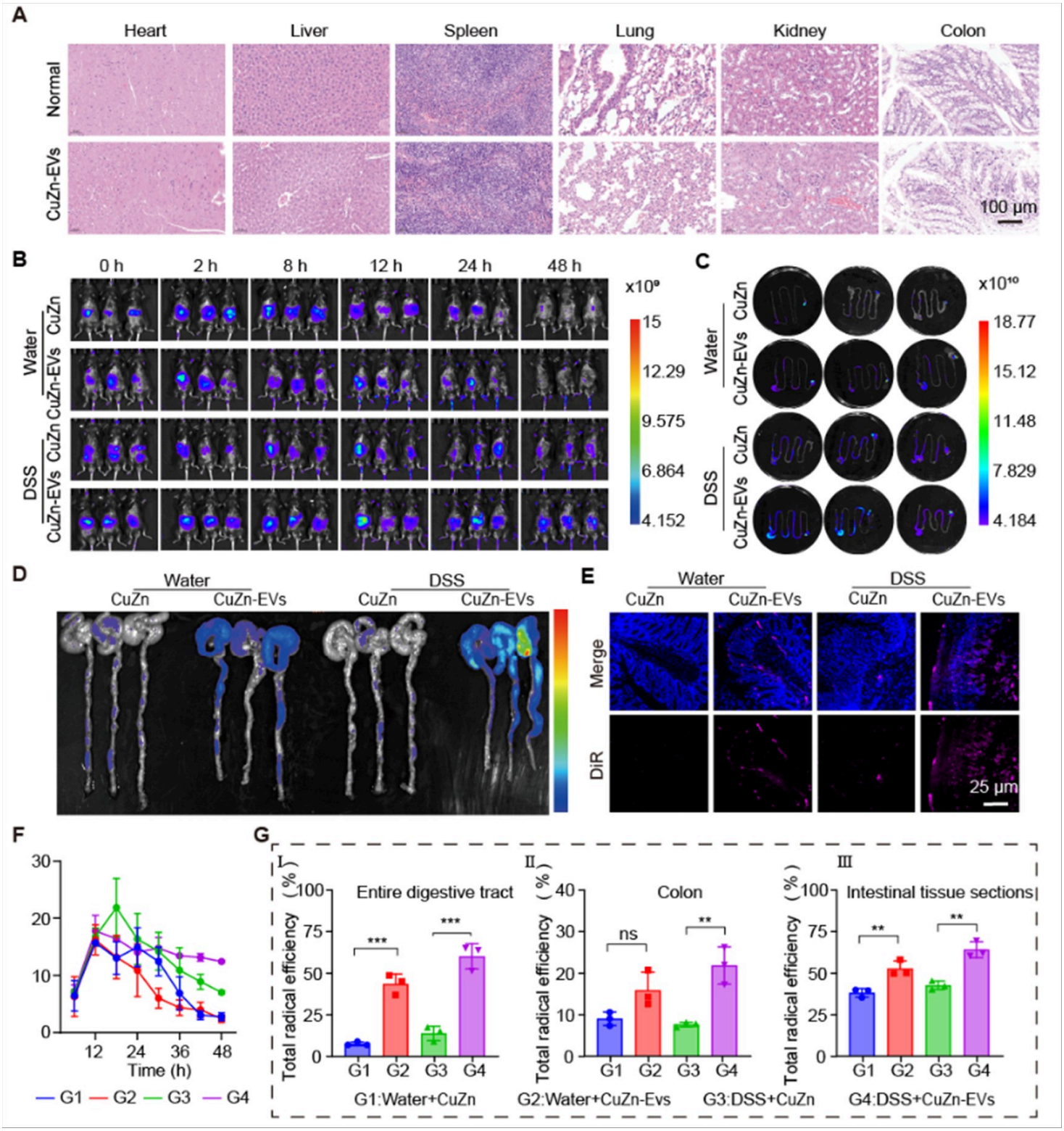


Figure 4

***In vivo*biosafety and intestinal targeting properties of CuZn-EVs.**

(A) Representative H&E staining images of major organs, including heart, liver, spleen, lung, kidney, and colon, after CuZn-EVs administration. Scale bars, 100 μm. (B) *In vivo*fluorescence imaging of mice after oral administration of DiR-labeled CuZn nanozymes and CuZn-EVs under normal or DSS-induced colitis

conditions at different time points (0 – 48 h). (C) Representative fluorescence imaging of the entire digestive tract after oral administration of CuZn nanozymes and CuZn-EVs in normal and DSS-treated mice. (D) *Ex vivo* fluorescence imaging of isolated gastrointestinal tissues from different treatment groups. (E) Fluorescence images of colon tissue sections showing the distribution and retention of DiR-labeled nanoparticles in colonic tissues. Nuclei were stained with DAPI. Scale bars, 25 μm. (F) Time-dependent fluorescence quantification of gastrointestinal retention after oral administration. (G–I) Quantitative analysis of fluorescence intensity in the entire digestive tract, colon, and intestinal tissue sections, respectively. Data are presented as mean ± SD (*n*= 3).

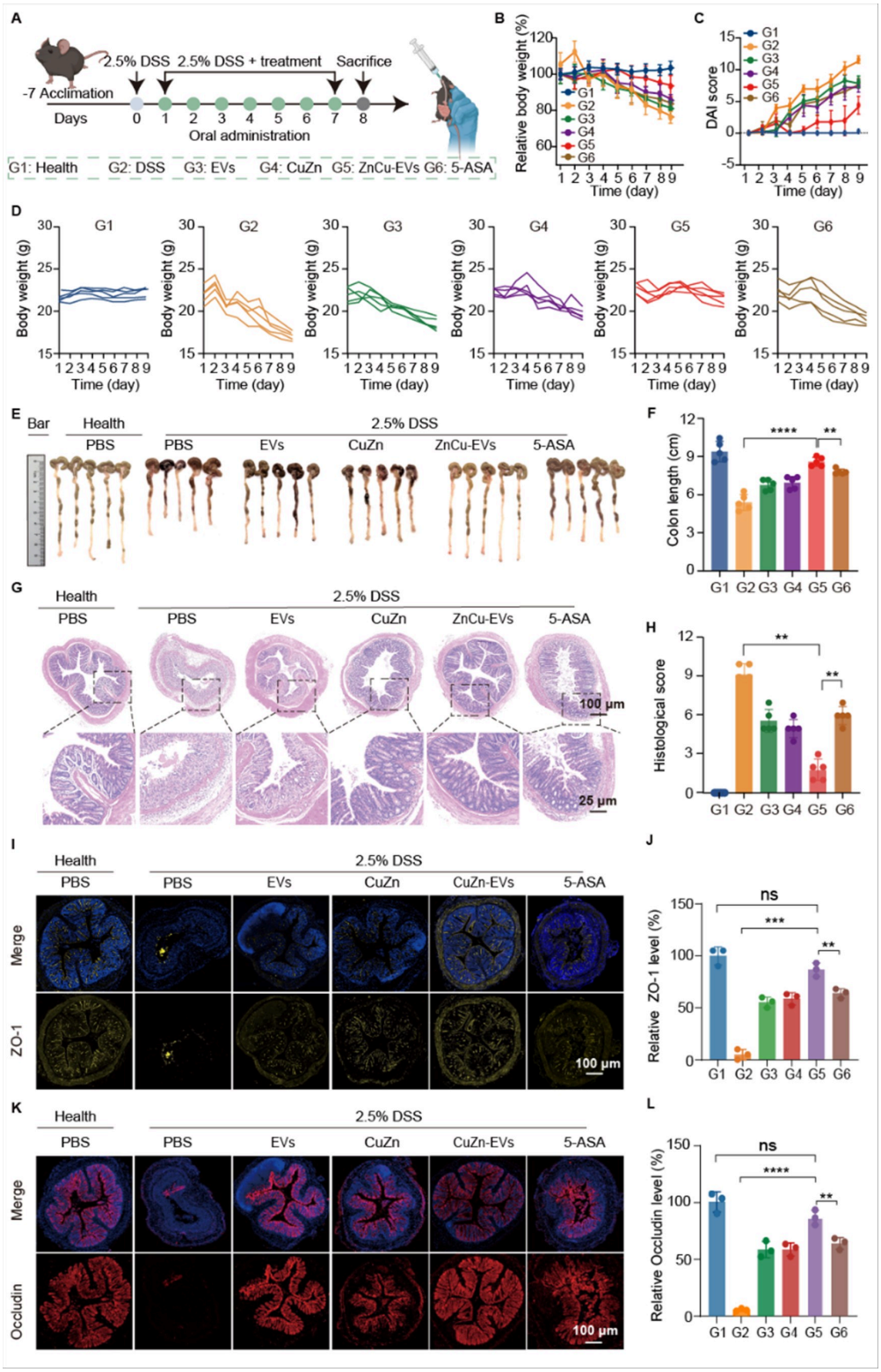


Figure 5

Therapeutic effects of CuZn-EVs in DSS-induced colitis mice. (A) Experimental design for DSS-induced colitis treatment with CuZn-EVs. Mice received 2.5% DSS followed by different therapeutic interventions. (B) Changes in relative body weight during disease progression. (C) DAI scores across treatment groups. (D) Individual body weight trajectories for each group. (E) Representative images of colons from different groups. (F) Quantification of colon length. (G) Representative H&E staining images of colon

tissues. Scale bars, 100 μm and 25μm. (H) Histological injury scores based on tissue pathology. (I) Immunofluorescence staining images of ZO-1 in colon sections; nuclei were counterstained with DAPI. Scale bars, 100 μm. (J) Quantitative analysis of ZO-1 fluorescence intensity. Data are presented as mean ± SD (*n* = 3). (K)Immunofluorescence of Occludin in colon tissues; nuclei were counterstained with DAPI. Scale bars, 100 μm. (L) Quantitative analysis of Occludin fluorescence intensity. Data are presented as mean ± SD (*n* = 3). Statistical analysis: one-way ANOVA; ns, not significant; **$p < 0.01$; ***$p<0.001$.

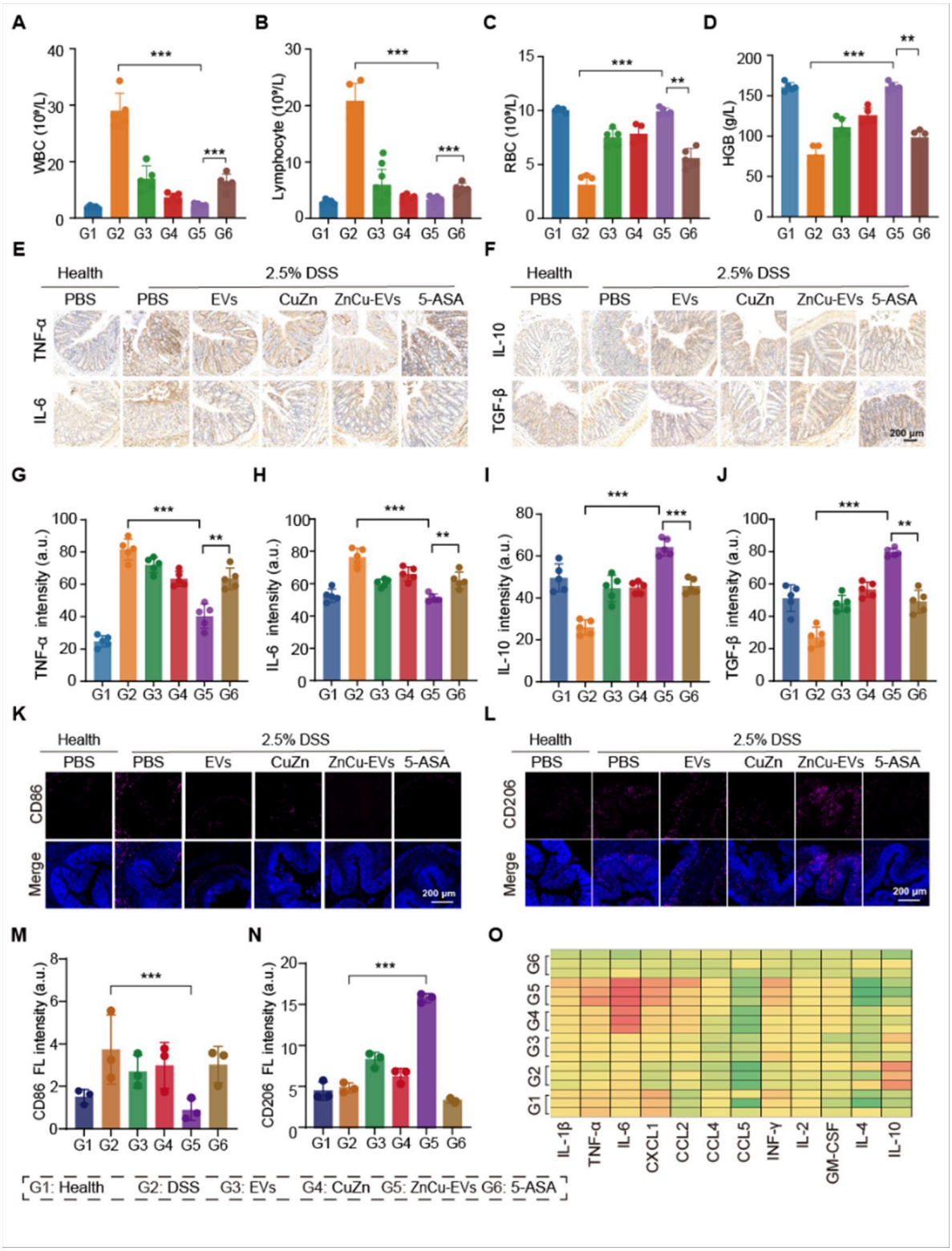


Figure 6

Quantification of inflammation regulation capacity of CuZn-EVs in colitis model.
(A–D) Hematological assessment of systemic inflammatory and injury markers, including WBC, lymphocyte, RBC counts, and hemoglobin levels across treatment groups. (E–F) Representative immunohistochemical staining images of pro-inflammatory cytokines (TNF-α, IL-6) and anti-inflammatory cytokines (IL-10, TGF-β) in colonic tissues. Scale bars, 200 μm. (G–J) Quantitative evaluation of TNF-α, IL-6, IL-10, and TGF-βexpression in colon samples. (K–L) Immunofluorescence detection of macrophage polarization markers CD86 (M1) and CD206 (M2) in colonic sections. Nuclei were counterstained with DAPI. Scale bars, 200 μm. (M–N) Quantification of CD86 and CD206 fluorescence intensities. (O) Heatmap representation of inflammatory cytokine expression patterns among different treatment groups. Data are expressed as mean ±SD (n = 3). Statistical differences were determined using one-way ANOVA. ns, not significant; *p < 0.05; **p < 0.01; ***p< 0.001.

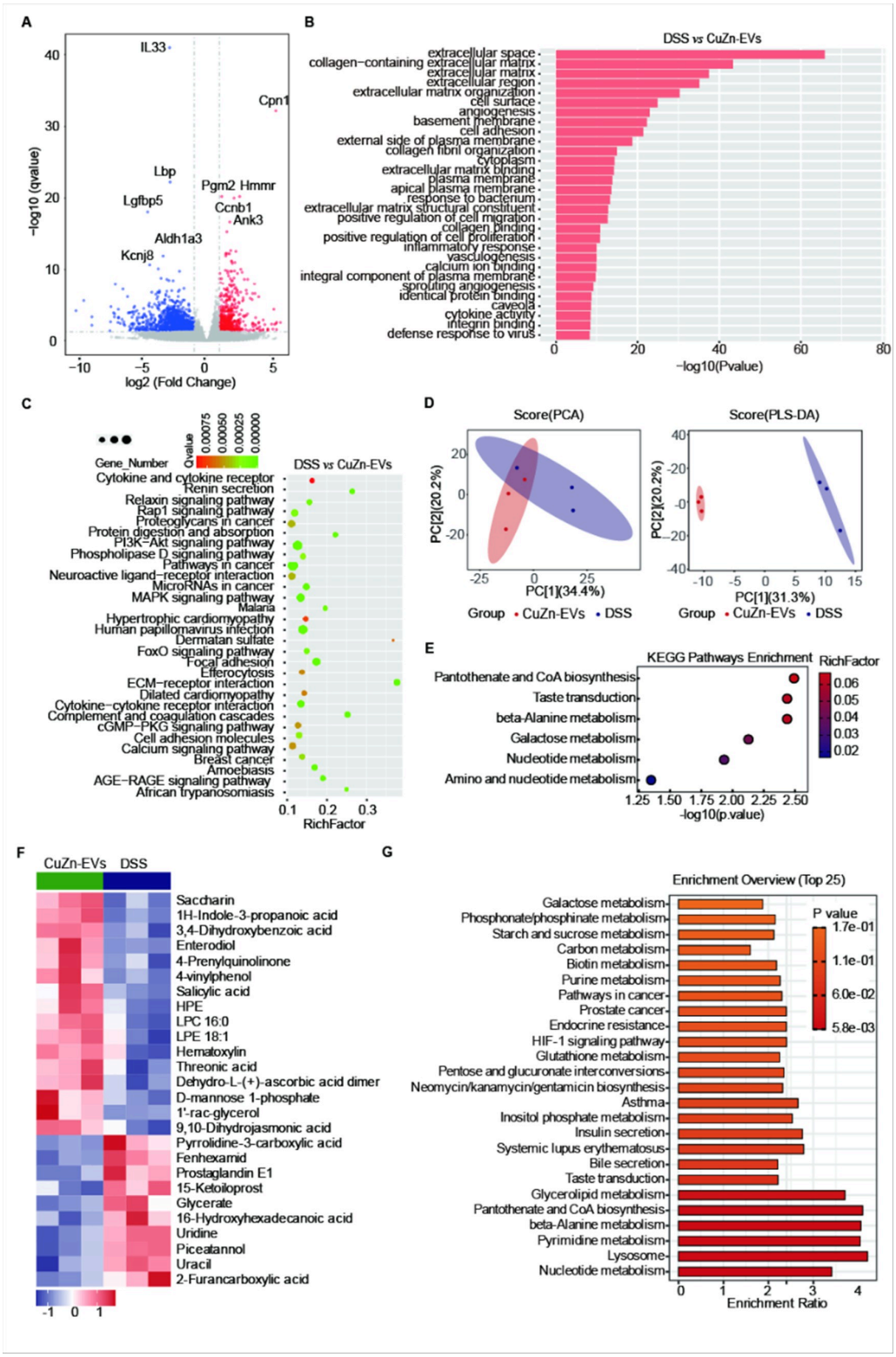


Figure 7

Multi-omics analyses of CuZn-EVs-mediated protection in experimental colitis.
(A) Differential gene expression profile comparing DSS-challenged mice with CuZn-EVs-treated animals. Upregulated and downregulated transcripts are indicated in red and blue, respectively. (B) GO-based functional classification of significantly altered transcripts. (C) KEGG-based pathway mapping of transcriptional changes. (D) PCA and PLS-DA score plots of metabolomic profiles between the CuZn-EVs

and DSS groups. (E) Pathway annotation of metabolites exhibiting significant abundance changes. (F) Clustered heatmap displaying representative metabolic features associated with CuZn-EVs administration. (G) Global overview of the major metabolic pathways influenced by treatment.

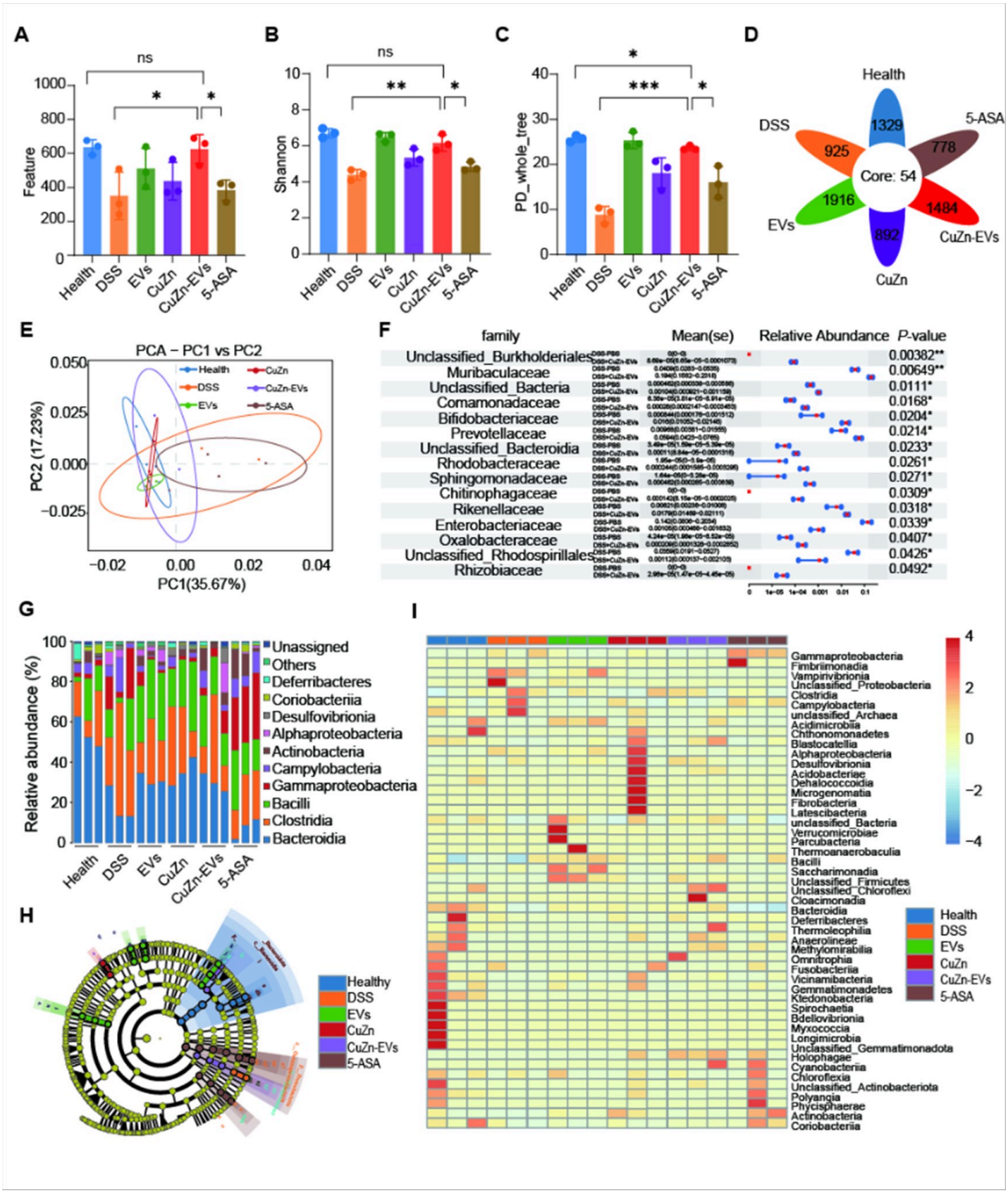


Figure 8

Gut microbial ecology in DSS-challenged and CuZn-EVs treated mice. (A–C) Evaluation of microbial diversity and richness using Feature richness, Shannon diversity, and PD whole-tree metrics. (D) Distribution of overlapping and group-specific OTUs among experimental cohorts. (E) Ordination analysis based on principal components demonstrating microbial community clustering patterns. (F) Differences in the abundance of dominant bacterial families among groups. (G) Phylum-level microbial composition across treatment conditions. (H) Discriminative microbial taxa identified by LEfSe analysis. (I) Heatmap visualization of bacterial taxa at the class rank. Data are presented as mean ± SD (n = 3). Statistical analyses were performed using one-way ANOVA. ns, no significance; *p < 0.05, **p < 0.01, ***p < 0.001.

Supplementary Files

This is a list of supplementary files associated with this preprint. Click to download.

- SupplementaryMaterials.docx
- supplementaryfile.docx